

Journal of Medical Imaging

MedicalImaging.SPIEDigitalLibrary.org

Study on structural atrophy changes and functional connectivity measures in Alzheimer's disease

Saraswathi Subramanian
Karunanithi Rajamanickam
Joy Sebastian Prakash
Murugesan Ramachandran
for Alzheimer's Disease Neuroimaging Initiative (ADNI)

SPIE.

Saraswathi Subramanian, Karunanithi Rajamanickam, Joy Sebastian Prakash, Murugesan Ramachandran for Alzheimer's Disease Neuroimaging Initiative (ADNI) "Study on structural atrophy changes and functional connectivity measures in Alzheimer's disease," *J. Med. Imag.* 7(1), 016002 (2020), doi: 10.1117/1.JMI.7.1.016002

Study on structural atrophy changes and functional connectivity measures in Alzheimer's disease

Saraswathi Subramanian, Karunanithi Rajamanickam,*
Joy Sebastian Prakash, and Murugesan Ramachandran[†]
for Alzheimer's Disease Neuroimaging Initiative (ADNI)

Chettinad Academy of Research and Education, Faculty of Allied Health Sciences,
Kelambakkam, Chennai, Tamil Nadu, India

Abstract. Alzheimer's disease (AD) is characterized by the progressive accumulation of neurofibrillary tangles associated with amyloid plaques. We used 80 resting-state functional magnetic resonance imaging and 80 T₁ images acquired using MP-RAGE (magnetization-prepared rapid acquisition gradient echo) from Alzheimer's Disease Neuroimaging Initiative data to detect atrophy changes and functional connectivity patterns of the default mode networks (DMNs). The study subjects were classified into four groups (each with $n = 20$) based on their Mini-Mental State Examination (MMSE) score as follows: cognitively normal (CN), early mild cognitive impairment, late mild cognitive impairment, and AD. The resting-state functional connectivity of the DMN was examined between the groups using the CONN functional connectivity toolbox. Loss of gray matter in AD was observed. Atrophy measured by the volume of selected subcortical regions, using the Functional Magnetic Resonance Imaging of the Brain (FMRIB) Software Library's Integrated Registration and Segmentation Tool (FIRST), revealed significant volume loss in AD when compared to CN ($p < 0.05$). DMNs were selected to assess functional connectivity. The negative connectivity of DMN increased in AD group compared to controls. Graph theory parameters, such as global and local efficiency, betweenness centrality, average path length, and cluster coefficient, were computed. Relatively higher correlation between MMSE and functional metrics ($r = 0.364$, $p = 0.001$) was observed as compared to atrophy measures ($r = 0.303$, $p = 0.006$). In addition, the receiver operating characteristic analysis showed large area under the curve (A_z) for functional parameters ($A_z > 0.9$), compared to morphometric changes ($A_z < 0.8$). In summary, it is observed that the functional connectivity measures may serve a better predictor in comparison to structural atrophy changes. We postulate that functional connectivity measures have the potential to evolve as a marker for the early detection of AD. © 2020 Society of Photo-Optical Instrumentation Engineers (SPIE) [DOI: [10.1117/1.JMI.7.1.016002](https://doi.org/10.1117/1.JMI.7.1.016002)]

Keywords: Alzheimer's disease; resting-state functional magnetic resonance imaging; default mode network; graph theory analysis.

Paper 19225R received Sep. 16, 2019; accepted for publication Feb. 3, 2020; published online Feb. 26, 2020.

1 Introduction

Alzheimer's disease (AD) accounts for more than 65% of dementia cases, characterized by progressive cognitive deficits, which include apraxia, differential impairment of recall memory, and language disturbances accompanied with other symptoms, such as psychosis, agitation, hallucinations, delusions, anxiety, and depression.¹⁻⁵ The progression of AD is due to several factors: severe tau-deposition and augmentation by oxidative damage, cholinergic neuronal death, beta-amyloid deposition, and microglial inflammation were found to be the cause of AD.⁶⁻⁹ The early stages of AD are determined by pathology in subjects with mild cognitive impairment

*Address all correspondence to Karunanithi Rajamanickam, E-mail: akrkaruna@gmail.com

[†]Data used in preparation of this article were obtained from the ADNI database (adni.loni.usc.edu). As such, the investigators within the ADNI contributed to the design and implementation of ADNI and/or provided data but did not participate in analysis or writing of this report. A complete listing of ADNI investigators can be found at: https://adni.loni.usc.edu/wp-content/uploads/how_to_apply/ADNI_Acknowledgement_List.pdf

(MCI), including the neurofibrillary tangles, plaques, and loss of basal forebrain cholinergic neurons.¹⁰ According to studies based on the AD pathogenesis, the accumulation of A β plaques in the brain is followed by the neurofibrillary tangles formation containing the tau protein, which results in the imbalance of A β plaque deposition.¹¹ The most commonly affected brain areas include the temporal lobe cortex and hippocampal regions with neurofibrillary tangles.¹² Gray matter loss in subjects with the cognitive decline has been found to be specific in cortical areas, such as the parietal, hippocampal, precuneus, and medial temporal lobes, resulting in high medial temporal atrophy.¹³ Recent studies reveal that evaluation of cerebrospinal fluid biomarkers using positron-emission tomography (PET) imaging has the ability to characterize the level of amyloid burden and the degree of neurodegenerative changes in AD patients.¹⁴

Brain morphometry using magnetic resonance imaging (MRI) is a well-known modality for the diagnosis and prognosis of AD.¹⁵ MRI of the brain can help effective visualization of the medial temporal lobe structures that are involved in MCI.¹⁶ Atrophy of hippocampus has been reported to be the most significant structural predictor involved in the conversion of MCI to AD.¹⁷ The most common structural MRI markers were the hippocampal and medial temporal atrophies, which are known to be involved in the progression of AD.¹⁸

Functional magnetic resonance imaging (fMRI) has made significant progress toward brain mapping and neural activity studies.¹⁹ The fMRI records the blood-oxygen-level-dependent (BOLD) signal changes with good spatial resolution to map the neuronal activity in the whole brain.²⁰ Resting-state functional magnetic resonance imaging (rs-fMRI) measures the low-frequency fluctuations (LFFs) (<0.1 Hz) to map spontaneous or intrinsic baseline neural activity as spatially consistent patterns.²¹ The functional resting-state networks (RSNs) were also acquired at these LFFs with the BOLD contrast. These LFFs are useful in interpreting the functional brain imaging outcome by measuring the regional neural activity in the RSNs.²² In AD patients, the fMRI studies of episodic memory show direct relevance to the early pathological changes in medial temporal and prefrontal cortices. Thus, in asymptomatic AD, fMRI serves as a useful tool for detecting the susceptible brain activity regions.²³ The rs-fMRI serves as a promising tool to understand and detect the functional connectivity of the brain by measuring the spontaneous LFFs in BOLD signals, which are temporally correlated across functionally related brain areas. This has led to the identification of various functionally correlated brain networks during the resting state.²⁴

Resting-state functional connectivity associated with major disconnections or alterations between several brain regions has been reported in various pathological cases, such as AD, multiple sclerosis, depression, and attention deficit hyperactivity disorder.²⁵ It has been suggested that the neuronal communications between the brain regions are associated with increased functional connectivity, due to the existence of neuroanatomical connections that prove that functionally linked brain networks reflect the underlying structural connectivity in various regions of the brain.²⁶ The anterior and posterior medial, lateral parietal cortex regions show intrinsic activity during rest as consistent pattern, known as default mode networks (DMNs). This type of functional network was found to be robust among cognitive states.²⁷ The rs-fMRI is also useful to study the relationship between brain activity and behavioral aspects. The graph-theory-based network analysis of rs-fMRI images has proved to be a potential tool to assess physiological mechanism of brain function.²⁸ The graph-theory-based network analysis computes several parameters to evaluate intrinsic or spontaneous brain connectivity network during neural disruptions and recovery.^{29–32}

MRI studies have independently reported atrophy and functional connectivity in the regions associated with DMNs and cognitive impairment in early mild cognitive impairment (EMCI), late mild cognitive impairment (LMCI), and AD. However, these studies lack demonstration of connectivity measures, such as degree centrality, clustering coefficients to provide better quantification of brain networks,³³ and disease conditions during cognitive impairment and AD.³⁴ Demonstration of the utility of a functional connectivity marker as a predicting factor is still lacking. In this study, an attempt is made to evaluate whether any correlation exists between atrophy, functional connectivity measures, and a commonly used clinical scoring method, viz., the Mini-Mental State Examination (MMSE) score. We hypothesize hypoconnectivity or hyperconnectivity of the functional associations in the DMNs and the metrics derived based on graph theory could serve as a predictive imaging marker in staging the disease.

Table 1 Age and MMSE of study groups.

Groups	Gender	Age (years) range	Age (mean \pm SD)	MMSE (mean \pm SD)	P-value (age)
CN ($N = 20$)	8 M, 12 F	65 to 95	76.85 \pm 7.46	28.75 \pm 1.34	—
EMCI ($N = 20$)	8 M, 12 F	56 to 82	70.90 \pm 6.56	27.80 \pm 1.83	CN versus EMCI: 0.010
LMCI ($N = 20$)	12 M, 8 F	58 to 87	70.50 \pm 7.19	27.95 \pm 1.32	EMCI versus LMCI: 0.855
AD ($N = 20$)	9 M, 11 F	56 to 87	73.40 \pm 7.57	22.60 \pm 2.46	LMCI versus AD: 0.221

2 Subjects and Methods

2.1 Subjects

The data used in this study were obtained from Alzheimer's Disease Neuroimaging Initiative (ADNI) database (adni.loni.usc.edu). The ADNI was led by Michael W. Weiner and was launched in the year 2003 with the aim to measure the progression of MCI and to differentiate from AD. ADNI uses imaging modalities, such as MRI, diffusion tensor imaging, PET, and other serum and cerebrospinal fluid biomarkers, along with clinical and neuropsychological assessment. The demographic data, such as age, gender, and occupation, are available for each patient. In this study, the cases were selected randomly from all the four groups [20 from each viz., cognitive normal (CN), EMCI, LMCI, and AD] based on the baseline screening from the ADNI website. Further, the demographic details, such as age, sex, MMSE, and clinical dementia rating (CDR) scores, were also recorded. Later, the neuropsychological assessment via MMSE score and CDR score were utilized to find the association with imaging parameters. Both structural [magnetization-prepared rapid acquisition gradient echo (MPRAGE)— T_1] and rs-fMRIs of the 80 subjects of the four different study groups, CN, EMCI, LMCI, and AD group patients, are analyzed (Table 1).

3 Methods

3.1 Image Acquisition Parameters

The MPRAGE sequence was used to acquire T_1 -weighted three-dimensional volume images for all the subjects. For T_1 images, the acquisition parameters are as follows: repetition time (TR)—2300 ms, echo time (TE)—3.1 ms, flip angle (FA)—9 deg, field of view (FOV)—93.75 mm², (number of phase and frequency encoding (acquisition matrix)—256 \times 240) and the slice thickness—1.2 mm. For the functional images, echo-planar imaging sequence was used with the following parameters: TR—3000 ms, TE—30 ms, FA—80 deg, number of slices—168, and the slice thickness—3 mm.

3.2 Structural Image Processing

The T_1 -weighted structural images were preprocessed (conversion of DICOM format to compressed four-dimensional NIFTI format) and then skull-stripped using brain extraction tool. The skull-stripped images were then processed with FIRST. In this step, the extracted regions (which generates *.nii file) are superimposed on the whole brain image of each subject to determine the accuracy of the segmentation and its anatomical position. The volumes of left and right regions of hippocampus, thalamus, amygdala, putamen, pallidum, caudate, and accumbens were measured and the represented in terms of volume (cubic millimeter).

3.3 Functional Image Processing

The functional images were processed using CONN toolbox, version 17.f (Ref. 35, RRID: SCR_009550) and statistical parametric mapping, version 8.³⁶ The standard preprocessing

pipeline includes realignment and slice timing correction. These realigned functional images were coregistered with the high-resolution structural T₁ image. The coregistered functional images were spatially normalized to Montreal Neurological Institute standard brain template and smoothed with 8 mm kernel. The functional data were denoised using CONN's default denoising method, which uses component-based noise reduction method—a combination of motion regression and scrubbing regressors. Later, using of bivariate correlation as a standard measure for functional connectivity analyses, and from the list of seeds/sources, the DMNs having 12 regions of interest (ROIs) were selected to perform the connectivity analyses. This performs the first-level analyses resulting in ROI-to-ROI connectivity matrices for each subject and for each condition. The graph theory measures of global efficiency, local efficiency, degree, cost, clustering coefficient, and average path length were also evaluated.

For functional assessments, regions associated with DMNs were selected. The default mode network consists of the precuneus, posterior cingulate cortex, the medial prefrontal cortex, inferior parietal lobe, and lateral and medial temporal cortex. Using bivariate correlation as a standard measure, functional connectivity between different ROIs was computed. From the list of seeds/sources, the DMNs, six ROIs viz., left and right of middle frontal gyrus, angular gyrus, posterior cingulate cortex, lateral parietal lobe, and parahippocampal and hippocampal regions were selected for connectivity analysis. The first-level analyses (slice time correction, motion correction, normalizing denoising, and smoothing) were performed between the above-mentioned ROI-to-ROI connectivity matrices ($2 \times 6 \times 6$) for controls and disease condition subject. In addition, the whole brain connectivity for 91 ROIs was carried out and the values are presented as mean and standard error in Table 2. The correlation maps were obtained and the graphical display of the ROI-to-ROI connectivity values for the between-subjects and between-condition contrasts were computed in the second-level analysis. Details of the seven parameters computed using graph theory²⁸ are as follows: global efficiency is the average of the inverse of the path length for all nodes. Local efficiency is the average global efficiency of subgraphs for each node containing the neighbors of that node. The degree is the simple measurement for the connectivity of a node with the rest of the nodes in a network. Average path length is the shortest path length between the nodes, which measures the network's capacity of transferring the information between the nodes. The measure betweenness centrality is a quantity of centrality in a graph based on the shortest path. Cost is the ratio of the existing number of edges to the number of all possible edges in the network. Clustering coefficients are the number of connections between the nearest neighbors of a node proportional to the maximum number of connections, whereas the mean of the clustering coefficients over all nodes is defined as the global clustering coefficient.³⁷

Table 2 Functional assessment at regions associated with DMNs [graph theory parameters (mean \pm SE)].

Graph theory parameters	CN ($N = 20$)	EMCI ($N = 20$)	LMCI ($N = 20$)	AD ($N = 20$)
Global efficiency	0.554 \pm 0.001	0.500 \pm 0.005*	0.509 \pm 0.003*	0.499 \pm 0.004*
Local efficiency	0.394 \pm 0.008	0.723 \pm 0.005*	0.729 \pm 0.004*	0.724 \pm 0.003*
Betweenness centrality	0.004 \pm 0.00	0.007 \pm 0.00*	0.007 \pm 0.00*	0.008 \pm 0.00*
Cost	0.150 \pm 0.00	0.150 \pm 0.00	0.150 \pm 0.00	0.150 \pm 0.00
Average path length	1.970 \pm 0.005	2.308 \pm 0.028*	2.242 \pm 0.017*	2.321 \pm 0.028*
Clustering coefficient	0.172 \pm 0.004	0.515 \pm 0.009*	0.511 \pm 0.007*	0.517 \pm 0.006*
Degree	24.45 \pm 0.000	24.45 \pm 0.000	24.45 \pm 0.000	24.45 \pm 0.000

*Represents significant reduction ($p < 0.05$) in the mean volume as compared to CN determined by *post-hoc* test.

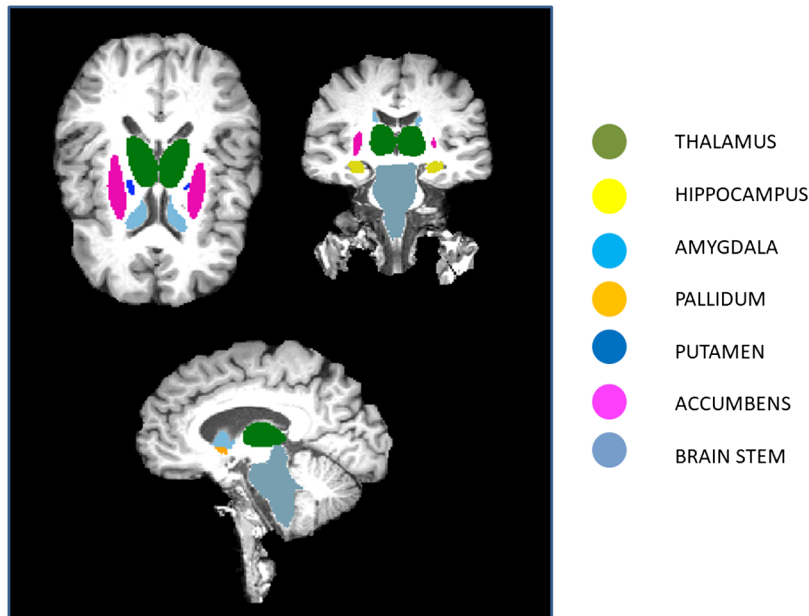


Fig. 1 Segmented color-coded ROIs.

4 Statistical Analysis

Statistical analysis was performed using Statistical Package for the Social Sciences Version 21 and the structural and functional parameters are expressed as mean and standard deviation. Computed structural volume of the ROIs and the functional metrics were subjected to analysis of variance (ANOVA) followed by Bonferroni *post-hoc* analysis. For intergroup comparison, Bonferroni adjusted *p*-values were used. Receiver operating characteristic curves were computed for CN and AD, and $p < 0.05$ was considered as statistically significant.

5 Results

The segmented anatomical regions color-coded and superimposed on the axial, sagittal, and coronal T₁-weighted image sections are presented in Fig. 1. Mean values of structural atrophy measures were compared between the study cohorts using ANOVA and *post-hoc* (Bonferroni) tests and the $p < 0.05$ was considered statistically significant (Tables 2 and 3). The structural and

Table 3 Morphometric assessment of volume in the selected ROIs.

ROIs	Volume (mm ³) (mean ± SE)			
	CN (N = 20)	EMCI (N = 20)	LMCI (N = 20)	AD (N = 20)
Hippocampus	3573.6 ± 76.2	2817.8 ± 257.8*	2848.0 ± 238*	2456.0 ± 217.8*
Thalamus	7001.8 ± 146.9	5696.3 ± 516.3*	6331.8 ± 402.4	5235.2 ± 488.4*
Amygdala	1205.9 ± 78.9	956.3 ± 96.5	1010.1 ± 69.8	878.8 ± 70.1
Putamen	4395.3 ± 116.9	3411.6 ± 334*	3765.8 ± 349.1	3031.9 ± 345.4*
Pallidum	1654.8 ± 67.3	1379.5 ± 134.5	1548.1 ± 133.1	1190.4 ± 119.1
Caudate	3366.8 ± 101.9	2701.4 ± 238.9*	2889.6 ± 255	2380.0 ± 269.6*
Accumbens	315.9 ± 19.9	302.1 ± 33.1	294.1 ± 32.6	276.3 ± 29.7

*Represents significant reduction ($p < 0.05$) in the mean volume as compared to CN determined by *post-hoc* test.

Table 4 Pearson's correlation coefficients of extracted imaging parameters with MMSE score.

ROIs for atrophy measure	Correlation to MMSE		Functional measures	Correlation to MMSE	
	<i>r</i>	<i>p</i>		<i>r</i>	<i>p</i>
Hippocampus	0.284	0.011	Global efficiency	0.342	0.002
Thalamus	0.303	0.006	Local efficiency	-0.352	0.001
Amygdala	0.221	0.049	Betweenness centrality	-0.364	0.001
Putamen	0.268	0.016	Cost	—*	—*
Pallidum	0.211	0.267	Average path length	0.336	0.002
Caudate	0.267	0.016	Clustering coefficient	-0.367	0.001
Accumbens	0.112	0.322	Degree	—*	—*

*Could not compute as the parameter is a constant.

functional parameters are represented as box plots (Figs. 2 and 3). The Pearson's correlation coefficient between the MMSE score and the structural and functional metrics are given in Table 4. The values of the area under the curve (AUC) are given in Table 5.

Functional connectivity with nodes and edges are presented in Fig. 4. The blue nodes with red edges represent the positive connectivity within the ROIs, whereas, the red nodes with blue edges represent the negative connectivity.

The functional connectograms for the study cohorts are displayed in Fig. 5. Functional measures, such as global, local efficiency, between centrality, path length, cluster coefficient, cost, and degree were assessed. The receiver operating characteristic curve (ROC) analysis (Fig. 6) was drawn for functional and structural atrophy changes, and the AUC with 95% confidence interval is presented in Table 5.

Table 5 Receiver operating characteristic curve analysis.

Test result variable(s)	AUC	95% confidence interval		<i>P</i> -value
		Lower bound	Upper bound	
Average path length	0.890	0.793	0.986	0.000
Betweenness centrality	0.619	0.482	0.755	0.114
Clustering coefficient	1.000	1.000	1.000	0.000
Local efficiency	0.881	0.778	0.983	0.000
Hippocampus	0.672	0.525	0.819	0.022
Thalamus	0.661	0.522	0.800	0.032
Amygdala	0.670	0.548	0.791	0.024
Putamen	0.665	0.531	0.799	0.028
Pallidum	0.664	0.529	0.800	0.029
Caudate	0.690	0.564	0.815	0.011
Accumbens	0.578	0.433	0.722	0.301

Bold values represent $p < 0.05$.

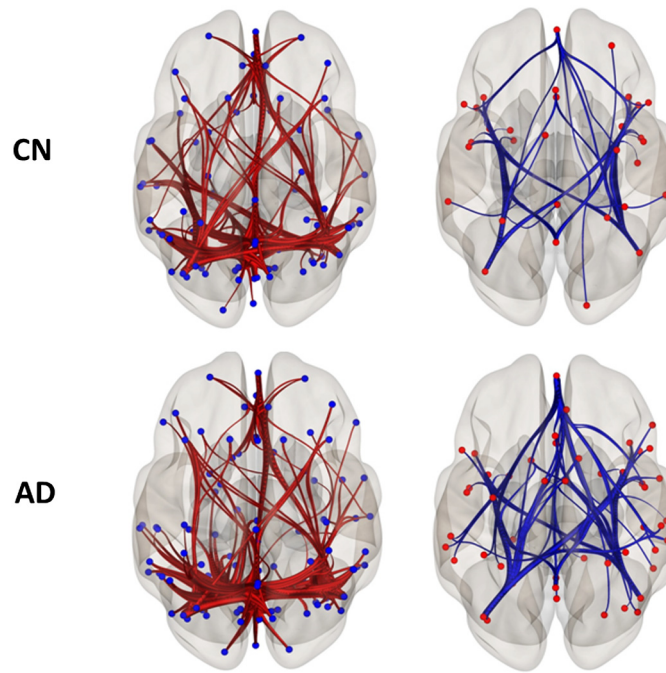


Fig. 4 Graph analysis—nodes and functional connections [ROI–ROI intrinsic functional connectivity (left—positive connectivity; right—negative connectivity)]. Red dots represent the nodes in each anatomic hemisphere; lines represent possible functional connections between those ROIs.

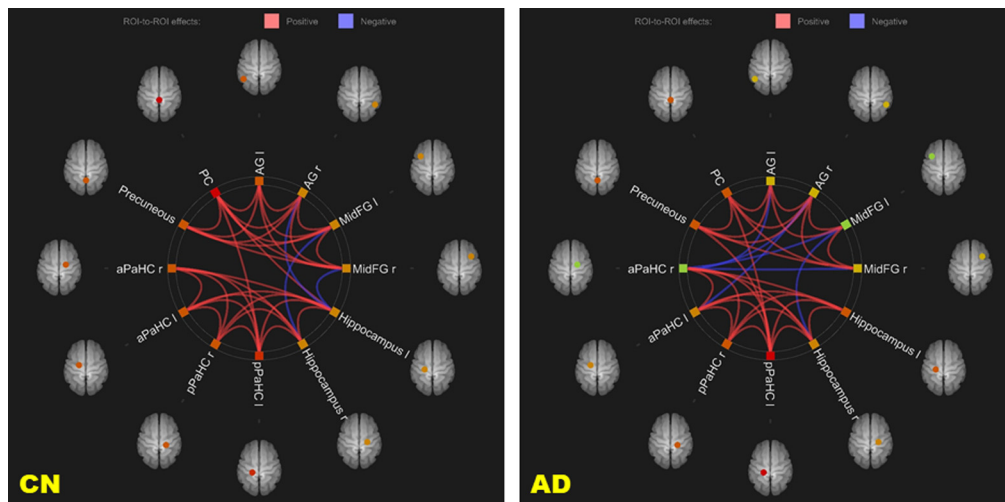


Fig. 5 Functional connectograms with positive (red) connectivity and negative (blue) connectivity.

6 Discussions

This study presents structural atrophy and functional connectivity measures in ADNI participants using MPRAGE T_1 -weighted and rs-fMRIs. Brain morphological variations, such as volume, thickness, and surface area, have been applied as a measure of structural association between brain regions.^{38,39} However, it is unclear how morphometric correlations relate to actual anatomical connectivity between brain regions. In the study cohorts, a decrease in volume in limbic regions, such as thalamus, hippocampus, in EMCI, LMCI, and AD groups, was observed, as compared to the controls. However, there was no significant reduction in the volumes in amygdala, pallidum, and accumbens. Previous studies have reported atrophy changes in

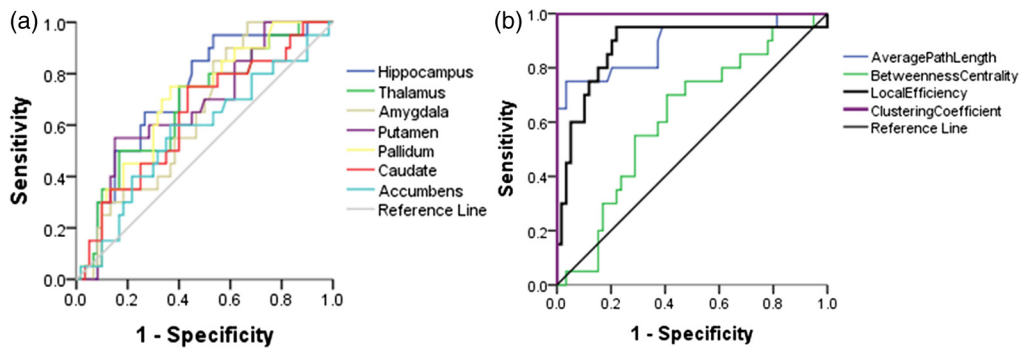


Fig. 6 ROC curves for (a) structural and (b) functional measures.

ROI, such as amygdala⁴⁰ and hippocampus,^{41–46} putamen and thalamus,⁴¹ and putamen, pallidum, and accumbens.^{40,41} These studies have postulated that atrophy or atrophy rate^{47,48} can serve as a strong predictive marker in demonstrating the progression of AD. However, a few other studies have reported that morphometric variations are not specifically related to AD.^{49,50} In another study, hippocampal atrophy, when correlated to MMSE yielded an r value of 0.21, a small positive correlation.⁴⁹ Clinical scoring methods are often subjective and dependent on clinical judgments and may not be fully adequate to recognize disease progression when used without any objective adjunct tools such as biochemical and imaging markers.^{50,51} Hence the functional objective biomarkers may facilitate an early as well as precise diagnosis of AD and complement the clinical criteria.

The pathophysiological effect of AD has been seen in the DMN regions, such as posterior cingulate cortex, lateral parietal cortex, and retrosplenial cortex in older patients with AD, associated with atrophy change (reduction in the volume) and metabolic abnormalities.⁵² In this study, functional connectivity analysis revealed a positive connectivity in AD as compared to CN. A similar finding has reported an increased functional connectivity at rest in left middle frontal gyrus in mild AD group.⁵³ Nevertheless, a decreased connectivity in the regions of thalamus and in the caudate has also been observed.⁵⁴ An increased connectivity in the DMNs was due to the deactivated structures in these networks.⁵⁵ Increased functional connectivity in the DMNs may also be due to a high level of amyloid deposition in AD leading to increased metabolic functioning in these regions.⁵⁶ The increased connectedness in AD may be interpreted as compensatory reallocation of cognitive possessions. These findings are in par with the earlier studies, which have reported higher DMN connectivity in AD.^{57–60} The posterior part of the DMN exhibited hyperconnectivity leading to the disturbance or dysfunction of switching from the rest to task condition.^{61,62}

Several studies have revealed that the change in the DMNs was accompanied with both the discrepancies and consistencies in MCI due to the clinical aspects of heterogeneity or by the methodological differences.⁶³ Theoretically, combining various MRI modalities, such as gray matter structure and functional connectivity measures, may produce more accurate classification than a single modality. A multimodal approach could provide complimentary information about different aspects of the disease. Our study revealed an increased classifying efficacy of functional measures, as compared to atrophy changes. Functional graph theory measures significantly classified disease condition (EMCI, LMCI, and AD), as compared to CN healthy controls. The functional connectivity graph theory method used in this study had specificity and sensitivity of 100% in classifying CN and AD. None of the AD was classified as CN and vice versa. This is a key feature of this functional assessment since classifying patients as healthy subject is a critical constraint in clinical applications.

7 Conclusion

There is continuous progress in the development of different methods and techniques to analyze the rs-fMRI data. Attempts to develop new processing techniques may be helpful in understanding the common or conflicting conclusions reported in the rs-fMRI literature.⁶⁴

In this work, the functional connectivity analysis using rs-fMRI offers greater sensitivity compared to conventional MRI-based atrophy measures to evaluate cognitive decline. In this study, we have observed structural atrophy in hippocampus, thalamus, amygdala, putamen, pallidum, and caudate in AD patients, in conformity with earlier studies. The rs-fMRI analysis showed an altered functional connectivity in EMCI, LMCI, and AD, as compared to CN. In this study, an increased functional connectivity in AD cohort is noted, which may be either due to compensational response or due to increased metabolic activity of amyloid plaques in AD. ROC analysis of the functional assessments gave improved predictive insight when compared to morphometric analysis, and thus establishes its utility as early predictor for clinical staging in cognitively impaired and AD patients. Increased number of study participants as well longitudinal studies may further validate these findings.

Disclosures

The authors have no relevant financial interests in the manuscript and no other potential conflicts of interest to disclose. This research was performed on Alzheimer's disease Neuroimaging Initiative database freely available for researchers, and hence no approval was required for animal care and use of committee protocol for human/animals and an institutional review board protocol for human data. K.R. designed the study; S.S. executed the study and generated the images and values for structural data; J.S.P. executed the study and generated the images and values for functional data; J.S.P., M.R., and K.R. prepared the article. All authors reviewed the article. The authors declare no competing financial interests and/or nonfinancial interests.

Acknowledgments

The authors would like to thank the Chettinad Academy of Research and Education (CARE) for a fellowship to research scholar Mr. Joy Sebastian Prakash, and the principal and faculty of Allied Health Sciences, CARE, for the immense support throughout the study. Data collection and sharing for this project was funded by the Alzheimer's Disease Neuroimaging Initiative (ADNI) (U.S. National Institutes of Health Grant No. U01 AG024904) and U.S. Department of Defense (DOD) ADNI Award (No. W81XWH-12-2-0012). ADNI is funded by the National Institute on Aging, the National Institute of Biomedical Imaging and Bioengineering, and through generous contributions from the following: AbbVie, Alzheimer's Association; Alzheimer's Drug Discovery Foundation; Araclon Biotech; BioClinica, Inc.; Biogen; Bristol-Myers Squibb Company; CereSpir, Inc.; Cogstate; Eisai Inc.; Elan Pharmaceuticals, Inc.; Eli Lilly and Company; EuroImmun; F. Hoffmann-La Roche, Ltd., and its affiliated company Genentech, Inc.; Fujirebio; GE Healthcare; IXICO Ltd.; Janssen Alzheimer Immunotherapy Research & Development, LLC.; Johnson & Johnson Pharmaceutical Research & Development LLC.; Lumosity; Lundbeck; Merck & Co., Inc.; Meso Scale Diagnostics, LLC.; NeuroRx Research; Neurotrack Technologies; Novartis Pharmaceuticals Corporation; Pfizer, Inc.; Piramal Imaging; Servier; Takeda Pharmaceutical Company; and Transition Therapeutics. The Canadian Institutes of Health Research provides funds to support ADNI clinical sites in Canada. Private sector contributions are facilitated by the Foundation for the National Institutes of Health. (www.fnih.org). The grantee organization is the Northern California Institute for Research and Education, and the study is coordinated by the Alzheimer's Therapeutic Research Institute at the University of Southern California. ADNI data disseminated by the Laboratory for Neuro Imaging at the University of Southern California are not applicable to this study as the data are downloaded from ADNI and only computational work was carried on in the author's laboratory. This research was for ADNI. Data used in preparation of this article were obtained from the ADNI database (adni.loni.usc.edu). As such, the investigators within the ADNI contributed to the design and implementation of ADNI and/or provided data but did not participate in analysis or writing of this report. A complete listing of ADNI investigators can be found at: https://adni.loni.usc.edu/wp-content/uploads/how_to_apply/ADNI_Acknowledgement_List.pdf.

References

1. R. S. Doody, P. Massman, and J. K. Dunn, "A method for estimating progression rates in Alzheimer disease," *Arch. Neurol.* **58**(3), 449–454 (2001).
2. K. G. Yiannopoulou and S. G. Papageorgiou, "Current and future treatments for Alzheimer's disease," *Ther. Adv. Neurol. Disord.* **6**(1), 19–33 (2012).
3. R. Mayeux and Y. Stern, "Epidemiology of Alzheimer disease," *Cold Spring Harbor Perspect. Med.* **2**(8), a006239 (2012).
4. R. E. Tanzi, "A genetic dichotomy model for the inheritance of Alzheimer's disease and common age-related disorders," *J. Clin. Invest.* **104**(9), 1175–1179 (1999).
5. C. Sassi et al., "Exome sequencing identifies 2 novel presenilin 1 mutations (p.L166V and p.S230R) in British early-onset Alzheimer's disease," *Neurobiol. Aging* **35**(10), 2422.e13–2422.e16 (2014).
6. T. Jiang, J. T. Yu, and L. Tan, "Novel disease-modifying therapies for Alzheimer's disease," *J. Alzheimers Dis.* **31**(3), 475–492 (2012).
7. M. N. Rossor et al., "The diagnosis of young-onset dementia," *Lancet Neurol.* **9**(8), 793–806 (2010).
8. L. L. Smits et al., "Early onset Alzheimer's disease is associated with a distinct neuropsychological profile," *J. Alzheimers Dis.* **30**(1), 101–108 (2012).
9. M. Roth, "The natural history of mental disorder in old age," *J. Mental Sci.* **101**(423), 281–301 (1955).
10. H. Braak and E. Braak, "Neuropathological staging of Alzheimer-related changes," *Acta Neuropathol.* **82**(4), 239–259 (1991).
11. J. Hardy and D. J. Selkoe, "The amyloid hypothesis of Alzheimer's disease: progress and problems on the road to therapeutics," *Science* **297**(5580), 353–356 (2002).
12. G. K. Wilcock and M. M. Esiri, "Plaques, tangles and dementia," *J. Neurol. Sci.* **56**(2), 343–356 (1982).
13. G. B. Frisoni et al., "The topography of grey matter involvement in early and late onset Alzheimer's disease," *Brain* **130**(3), 720–730 (2007).
14. W. E. Klunk et al., "Imaging brain amyloid in Alzheimer's disease with Pittsburgh Compound-B," *Ann. Neurol.* **55**(3), 306–319 (2004).
15. C. Plant et al., "Automated detection of brain atrophy patterns based on MRI for the prediction of Alzheimer's disease," *NeuroImage* **50**(1), 162–174 (2010).
16. L. Ferrarini et al., "Morphological hippocampal markers for automated detection of Alzheimer's disease and mild cognitive impairment converters in magnetic resonance images," *J. Alzheimers Dis.* **17**(3), 643–659 (2009).
17. L. G. Apostolova et al., "Conversion of mild cognitive impairment to Alzheimer disease predicted by hippocampal atrophy maps," *Arch. Neurol.* **63**(5), 693–699 (2006).
18. C. R. Jack, Jr. et al., "Prediction of AD with MRI-based hippocampal volume in mild cognitive impairment," *Neurology* **52**(7), 1397–1403 (1999).
19. N. K. Logothetis, "The neural basis of the blood-oxygen-level-dependent functional magnetic resonance imaging signal," *Philos. Trans. R. Soc. London Ser. B* **357**(1424), 1003–1037 (2002).
20. N. K. Logothetis, "MR imaging in the non-human primate: studies of function and of dynamic connectivity," *Curr. Opin. Neurobiol.* **13**(5), 630–642 (2003).
21. P. Fransson, "Spontaneous low-frequency BOLD signal fluctuations: an fMRI investigation of the resting-state default mode of brain function hypothesis," *Hum. Brain Mapping* **26**(1), 15–29 (2005).
22. M. De Luca et al., "fMRI resting state networks define distinct modes of long-distance interactions in the human brain," *NeuroImage* **29**(4), 1359–1367 (2006).
23. B. Desgranges, J. C. Baron, and F. Eustache, "The functional neuroanatomy of episodic memory: the role of the frontal lobes, the hippocampal formation, and other areas," *NeuroImage* **8**(2), 198–213 (1998).
24. S. Ogawa et al., "Intrinsic signal changes accompanying sensory stimulation: functional brain mapping with magnetic resonance imaging," *Proc. Natl. Acad. Sci. U.S.A.* **89**(13), 5951–5955 (1992).

25. L. Wang et al., “Changes in hippocampal connectivity in the early stages of Alzheimer’s disease: evidence from resting state fMRI,” *NeuroImage* **31**(2), 496–504 (2006).
26. M. P. van den Heuvel et al., “Functionally linked resting-state networks reflect the underlying structural connectivity architecture of the human brain,” *Hum. Brain Mapping* **30**(10), 3127–3141 (2009).
27. M. E. Raichle et al., “A default mode of brain function,” *Proc. Natl. Acad. Sci. U.S.A.* **98**(2), 676–682 (2001).
28. J. Wang, X. Zuo, and Y. He, “Graph-based network analysis of resting-state functional MRI,” *Front. Syst. Neurosci.* **4**, 16 (2010).
29. W. de Haan et al., “Functional neural network analysis in frontotemporal dementia and Alzheimer’s disease using EEG and graph theory,” *BMC Neurosci.* **10**, 101–101 (2009).
30. D. S. Bassett and E. T. Bullmore, “Human brain networks in health and disease,” *Curr. Opin. Neurol.* **22**(4), 340–347 (2009).
31. E. Bullmore and O. Sporns, “Complex brain networks: graph theoretical analysis of structural and functional systems,” *Nat. Rev. Neurosci.* **10**(3), 186–198 (2009).
32. Y. He et al., “Neuronal networks in Alzheimer’s disease,” *Neuroscientist* **15**(4), 333–350 (2009).
33. S. J. Son, J. Kim, and H. Park, “Structural and functional connective fingerprints in mild cognitive impairment and Alzheimer’s disease patients,” *PLoS One* **12**(3), e0173426 (2017).
34. X. Zhou et al., “Aberrant functional connectivity and structural atrophy in subcortical vascular cognitive impairment: relationship with cognitive impairments,” *Front. Aging Neurosci.* **8**, 14 (2016).
35. S. Whitfield-Gabrieli and A. Nieto-Castanon, “Conn: A functional connectivity toolbox for correlated and anticorrelated brain networks,” *Brain Connect.* **2**(3), 125–141 (2012).
36. W. D. Penny et al., Eds., *Statistical Parametric Mapping: The Analysis of Functional Brain Images*, Elsevier (2011).
37. C. Bernard et al., “PCC characteristics at rest in 10-year memory decliners,” *Neurobiol. Aging* **36**(10), 2812–2820 (2015).
38. Y. He, Z. Chen, and A. Evans, “Structural insights into aberrant topological patterns of large-scale cortical networks in Alzheimer’s disease,” *J. Neurosci.* **28**(18), 4756–4766 (2008).
39. L. Zhou et al., “Hierarchical anatomical brain networks for MCI prediction: revisiting volumetric measures,” *PLoS One* **6**(7), e21935 (2011).
40. S. P. Poulin et al., “Amygdala atrophy is prominent in early Alzheimer’s disease and relates to symptom severity,” *Psychiatry Res.* **194**(1), 7–13 (2011).
41. P. Eustache et al., “Multimodal magnetic resonance imaging in Alzheimer’s disease patients at prodromal stage,” *J. Alzheimers Dis.* **50**(4), 1035–1050 (2016).
42. J. P. Aggleton et al., “Thalamic pathology and memory loss in early Alzheimer’s disease: moving the focus from the medial temporal lobe to Papez circuit,” *Brain* **139**(7), 1877–1890 (2016).
43. C. Hahn et al., “Thalamic shape and cognitive performance in amnesic mild cognitive impairment,” *Psychiatry Invest.* **13**(5), 504–510 (2016).
44. L. W. de Jong et al., “Strongly reduced volumes of putamen and thalamus in Alzheimer’s disease: an MRI study,” *Brain* **131**(12), 3277–3285 (2008).
45. Z. Yao et al., “Analysis of gray matter in AD patients and MCI subjects based voxel-based morphometry,” *Lect. Notes Comput. Sci.* **6889** (2011).
46. W. J. P. Henneman et al., “Hippocampal atrophy rates in Alzheimer disease: added value over whole brain volume measures,” *Neurology* **72**(11), 999–1007 (2009).
47. J. Barnes et al., “A meta-analysis of hippocampal atrophy rates in Alzheimer’s disease,” *Neurobiol. Aging* **30**(11), 1711–1723 (2009).
48. J. D. Sluimer et al., “Whole-brain atrophy rate and cognitive decline: longitudinal MR study of memory clinic patients,” *Radiology* **248**(2), 590–598 (2008).
49. A. M. Fjell et al., “Mini-Mental State Examination is sensitive to brain atrophy in Alzheimer’s disease,” *Dementia Geriatr. Cognit. Disord.* **28**(3), 252–258 (2009).

50. I. Arevalo-Rodriguez et al., "Mini-mental state examination (MMSE) for the detection of Alzheimer's disease and other dementias in people with mild cognitive impairment (MCI)," *Cochrane database Syst. Rev.* (3), CD010783 (2015).
51. J. A. Lonie, K. M. Tierney, and K. P. Ebmeier, "Screening for mild cognitive impairment: a systematic review," *Int. J. Geriatr. Psychiatry* **24**(9), 902–915 (2009).
52. R. L. Buckner et al., "Molecular, structural, and functional characterization of Alzheimer's disease: evidence for a relationship between default activity, amyloid, and memory," *J. Neurosci.* **25**(34), 7709–7717 (2005).
53. R. Balachandar et al., "A study of structural and functional connectivity in early Alzheimer's disease using rest fMRI and diffusion tensor imaging," *Int. J. Geriatr. Psychiatry* **30**(5), 497–504 (2015).
54. E. R. Kenny et al., "Subcortical connectivity in dementia with Lewy bodies and Alzheimer's disease," *Br. J. Psychiatry* **203**(3), 209–214 (2013).
55. C. L. Grady et al., "Age-related changes in brain activity across the adult lifespan," *J. Cognit. Neurosci.* **18**(2), 227–241 (2006).
56. R. L. Buckner, J. R. Andrews-Hanna, and D. L. Schacter, "The brain's default network: anatomy, function, and relevance to disease," *Ann. N.Y. Acad. Sci.* **1124**, 1–38 (2008).
57. E. L. Dennis and P. M. Thompson, "Functional brain connectivity using fMRI in aging and Alzheimer's disease," *Neuropsychol. Rev.* **24**(1), 49–62 (2014).
58. K. Wang et al., "Altered functional connectivity in early Alzheimer's disease: a resting-state fMRI study," *Hum. Brain Mapping* **28**(10), 967–978 (2007).
59. C. L. Grady et al., "Altered brain functional connectivity and impaired short-term memory in Alzheimer's disease," *Brain* **124**(4), 739–756 (2001).
60. C. L. Grady et al., "Evidence from functional neuroimaging of a compensatory prefrontal network in Alzheimer's disease," *J. Neurosci.* **23**(3), 986–993 (2003).
61. K. Ishibashi et al., "Altered functional connectivity of the default mode network by glucose loading in young, healthy participants," *BMC Neurosci.* **19**(1), 33 (2018).
62. T. Hedden et al., "Disruption of functional connectivity in clinically normal older adults harboring amyloid burden," *J. Neurosci.* **29**(40), 12686–12694 (2009).
63. F. Bai et al., "Default-mode network activity distinguishes amnesic type mild cognitive impairment from healthy aging: a combined structural and resting-state functional MRI study," *Neurosci. Lett.* **438**(1), 111–115 (2008).
64. H. Lv et al., "Resting-state functional MRI: everything that nonexperts have always wanted to know," *AJNR Am. J. Neuroradiol.* **39**(8), 1390–1399 (2018).
65. www.fnih.org.

Saraswathi Subramanian attained her master's degree in medical biotechnology from Chettinad Academy of Research and Education, Kelambakkam, Chennai, India. She is currently working as research assistant at the Translational Research Platform for Veterinary Biologicals (TRPVB) at Taminadu Veterinary and Animal Sciences University (TANUVAS), Chennai, India.

Karunanithi Rajamanickam is presently working as an associate professor at Chettinad Academy of Research and Education, India. He worked as a postdoctoral researcher at the Ottawa Hospital and Research Institute (OHRI), University of Ottawa, Canada, for three years after his completion of doctoral program in the Department of Medical Physics, Anna University, India. His research interest includes medical image analysis, MRI, diffusion tensor imaging, fMRI, and T1 and T2 MR mapping studies. He is passionate in computer programming languages such as MATLAB and FORTRAN.

Joy SebastianPrakash attained his PhD from Chettinad Academy of Research and Education, Kelambakkam, Chennai, India. He attained his master of philosophy (MPhil) and master of science (MSc) in biotechnology from St. Joseph's College (Autonomous), Tiruchirappalli, Tamil Nadu, India, and Bachelor of Science (BSc) in biotechnology from Dr. M.G.R University, Maduravoyal, Chennai, India. His research interest includes developing functionalized nanoprobes using quantum dots for biological imaging.

Murugesan Ramachandran is currently working as director of research at the Chettinad Academy of Research and Education, Kelambakkam, Chennai, India. He was a professor emeritus at the Networking Resource Centre in Biological Sciences, Madurai Kamaraj University, Madurai, India. His postdoctoral research was in study of magnetic ordering and spin diffusion in low dimensional magnetic materials by ESR with Prof. E. de Boer—University of Nijmegen, The Netherlands. His research interest includes medical imaging, artificial intelligence in medicine, bioinformatics and drug discovery, biomarker discovery, low-cost diagnostic kit development, biomaterials, biomedical magnetic resonance, nanomedicine, and photodynamic therapy.